1985

Nuclear Engineering and Design 86 (1985) 369–381
North-Holland, Amsterdam

THERMAL RESISTANCE OF CYLINDER-FLAT CONTACTS: THEORETICAL ANALYSIS AND EXPERIMENTAL VERIFICATION OF A LINE-CONTACT MODEL

G.R. McGEE [1], M.H. SCHANKULA [1] and M.M. YOVANOVICH [2]

[1] *Atomic Energy of Canada Limited Research Company, Whiteshell Nuclear Research Establishment, Pinawa, Manitoba ROE 1L0, Canada*

[2] *Professor, Mechanical Engineering, University of Waterloo, Waterloo, Ontario N2L 3G1, Canada*

Received 25 July 1984

A line-contact model for the thermal resistance of a cylinder-flat contact is presented. Resistance due to heat flow constriction across the solid-to-solid contact is calculated. The model also accounts for the variation in resistance across the gas-filled gap, on either side of the contact, as a function of gas pressure.

Experimental measurements of the overall thermal resistance were performed in helium and argon, at pressures between 10^{-6} Torr and atmospheric. The effect of contact pressure was investigated for mechanical loads between 80 N and 8000 N on specimens fabricated from Keewatin tool steel, Type 304 stainless steel and Zircaloy-4.

The experimental data were compared with the model predictions, and good agreement was obtained over a limited range of experimental parameters. The implications of slight amounts of form error (crowning) along the contacting surfaces are also discussed.

1. Introduction

There exists, within the nuclear industry, a class of heat-transfer problems for which it is important to know the thermal constriction and gap resistance between two right-circular cylinders contacting along their longitudinal axes.

To cite one example, the fuel and coolant in a CANDU-PHW reactor are separated from the moderator by a fuel channel, which consists of a pressure tube separated from a surrounding concentric calandria tube by a gas-filled (CO_2 or N_2) gap. An important feature of this system is that the cool heavy-water moderator surrounding each horizontal fuel channel can act as a sink for the heat generated during and after a severe loss-of-coolant accident.

In the event of such an accident, high temperatures in the fuel and pressure tube result in the pressure tube sagging into contact with the bottom of the calandria tube. The rate of heat release to the moderator will depend, in part, on the thermal resistance of the pressure tube/calandria tube interface. Accurate predictions of the constriction and gap resistance for this situation are required for reactor safety analysis [1].

This paper presents an analytical and experimental study of the constriction and gap resistance for the line contact formed between a right circular cylinder and a smooth parallel flat. (The flat represents a calandria tube with an infinite radius of curvature). Mathematical models are presented for the resistance to heat flow through the solid-to-solid line contact and through the surrounding gas-filled gap. The relevant geometrical and thermophysical parameters are expressed in dimensionless form, and their relative importance in controlling the heat transfer across the cylinder-flat contact is assessed.

A series of experiments to test the validity of these models is also described. Thermal experiments were performed on several materials (tool steel, stainless steel, and zirconium alloys) in vacuum and in helium and argon at pressures up to atmospheric. The experimental apparatus, the test procedure, the experimental results, and comparisons of the results with theoretical predictions are described.

2. Analysis

The thermal resistance of a joint consisting of a smooth right circular cylinder in contact with a smooth flat surface is analyzed. The upper and lower boundaries of the joint are isothermal planes parallel to the contact

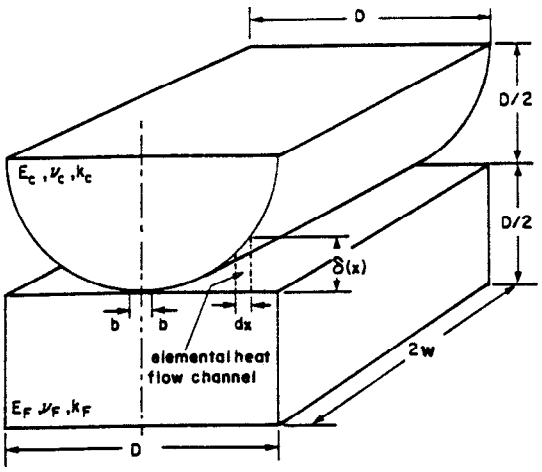

Fig. 1. Cylinder-flat contact geometry.

plane, spaced one diameter (D) apart (see fig. 1). Four adiabatic planes normal to the contact plane form the rectangular crosssection, of length $2w$ and width D. A static load, N, causes a line contact of width $2b$ to be formed between the cylindrical surface and the flat surface.

2.1 Constriction resistance for a line contact

Following an elastic plane strain analysis [2,3], the contact width, $2b$, between a cylinder and a flat is given by

$$2b = (16N\Delta D/2w\pi)^{1/2}, \tag{1}$$

where N is the normal load and Δ is the effective combined modulus expressed in terms of Young's modulus, E, and Poisson's ratio, ν, as

$$\Delta = \tfrac{1}{2}\left[\left(\frac{1-\nu_C^2}{E_C}\right)+\left(\frac{1-\nu_F^2}{E_F}\right)\right]. \tag{2}$$

Alternatively, the contact size may be expressed in terms of a non-dimensional load, L, as

$$\frac{1}{L} = \frac{2b}{D} = 4\left(\frac{N^*}{\pi}\right)^{1/2}, \tag{3}$$

where

$$N^* = N\Delta/2wD. \tag{4}$$

Given this expression for the contact width in terms of the cylinder-flat geometry, normal load, and material properties, the overall thermal constriction resistance is obtained by addition of the separate resistances for the cylinder and flat, respectively.

The constriction resistance for an isothermal strip contact, of width $2b$, placed on the surface of a half-cylinder is obtained from the full-cylinder solution of Yovanovich and Coutanceau [4], and is given by

$$R_C = \frac{1}{2w\pi k_C}\ln\left(\frac{2D}{b}\right) - \frac{1}{4wk_C}, \tag{5}$$

where k_C is the thermal conductivity of the cylinder.

An expression for the constriction resistance of a line contact of width $2b$, on the surface of a flat, was derived by Veziroglu and Chandra [5] and is given by

$$R_F = \frac{1}{2w\pi k_F}\ln\left(\frac{D}{\pi b}\right), \tag{6}$$

where k_F is the thermal conductivity of the flat.

The overall thermal resistance, R_c, of the solid-to-solid line contact is the sum of R_C and R_F, and, making use of eq. (3), is expressed as

$$R_c = \frac{1}{4w}\frac{1}{\pi k_C}\ln\left(\frac{\pi}{N^*}\right) - \frac{1}{k_C} + \frac{1}{\pi k_F}\ln\left(\frac{1}{4\pi N^*}\right). \tag{7}$$

A dimensionless constriction resistance $R_c^* = 2wk_sR_c$ may be formulated in terms of the harmonic mean thermal conductivity, k_s, as

$$R_c^* = \frac{k_s}{k_C}\frac{1}{2\pi}\ln\left(\frac{\pi}{N^*}\right) - \frac{k_s}{2k_C} + \frac{k_s}{k_F}\frac{1}{2\pi}\ln\left(\frac{1}{4\pi N^*}\right), \tag{8}$$

where

$$k_s = \frac{2k_Ck_F}{k_C+k_F}. \tag{9}$$

If $k_C = k_F = k_s$, then

$$R_c^* = \left(\frac{1}{\pi}\right)\ln\left(\frac{1}{N^*}\right) - 0.7206. \tag{10}$$

2.2 Resistance of the gas-filled gap

The thermal resistance of the gas-filled gap depends on three local quantities: the separation of the two solid bounding surfaces, the thermal conductivity of the gas, and the temperature difference between the surfaces.

The gap is divided into elemental heat flow channels having isothermal upper and lower surfaces, and adiabatic sides (see fig. 1). The heat flow lines in each channel are assumed to be straight and perpendicular to the plane of contact, which is a reasonable assumption near the line contact where the two solid surfaces are

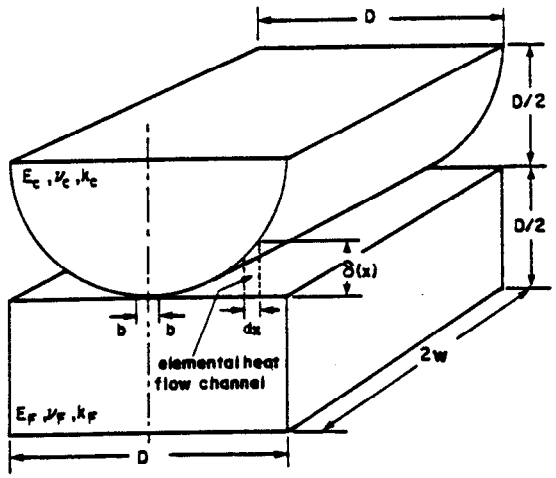

Fig. 1. Cylinder-flat contact geometry.

plane, spaced one diameter (D) apart (see fig. 1). Four adiabatic planes normal to the contact plane form the rectangular crosssection, of length $2w$ and width D. A static load, N, causes a line contact of width $2b$ to be formed between the cylindrical surface and the flat surface.

2.1 Constriction resistance for a line contact

Following an elastic plane strain analysis [2,3], the contact width, $2b$, between a cylinder and a flat is given by

$$2b = (16N\Delta D/2w\pi)^{1/2}, \tag{1}$$

where N is the normal load and Δ is the effective combined modulus expressed in terms of Young's modulus, E, and Poisson's ratio, ν, as

$$\Delta = \tfrac{1}{2}\left[\left(\frac{1-\nu_C^2}{E_C}\right)+\left(\frac{1-\nu_F^2}{E_F}\right)\right]. \tag{2}$$

Alternatively, the contact size may be expressed in terms of a non-dimensional load, L, as

$$\frac{1}{L} = \frac{2b}{D} = 4\left(\frac{N^*}{\pi}\right)^{1/2}, \tag{3}$$

where

$$N^* = N\Delta/2wD. \tag{4}$$

Given this expression for the contact width in terms of the cylinder-flat geometry, normal load, and material properties, the overall thermal constriction resistance is obtained by addition of the separate resistances for the cylinder and flat, respectively.

The constriction resistance for an isothermal strip contact, of width $2b$, placed on the surface of a half-cylinder is obtained from the full-cylinder solution of Yovanovich and Coutanceau [4], and is given by

$$R_C = \frac{1}{2w\pi k_C}\ln\left(\frac{2D}{b}\right) - \frac{1}{4wk_C}, \tag{5}$$

where k_C is the thermal conductivity of the cylinder.

An expression for the constriction resistance of a line contact of width $2b$, on the surface of a flat, was derived by Veziroglu and Chandra [5] and is given by

$$R_F = \frac{1}{2w\pi k_F}\ln\left(\frac{D}{\pi b}\right), \tag{6}$$

where k_F is the thermal conductivity of the flat.

The overall thermal resistance, R_c, of the solid-to-solid line contact is the sum of R_C and R_F, and, making use of eq. (3), is expressed as

$$R_c = \frac{1}{4w}\frac{1}{\pi k_C}\ln\left(\frac{\pi}{N^*}\right) - \frac{1}{k_C} + \frac{1}{\pi k_F}\ln\left(\frac{1}{4\pi N^*}\right). \tag{7}$$

A dimensionless constriction resistance $R_c^* = 2wk_sR_c$ may be formulated in terms of the harmonic mean thermal conductivity, k_s, as

$$R_c^* = \frac{k_s}{k_C}\frac{1}{2\pi}\ln\left(\frac{\pi}{N^*}\right) - \frac{k_s}{2k_C} + \frac{k_s}{k_F}\frac{1}{2\pi}\ln\left(\frac{1}{4\pi N^*}\right), \tag{8}$$

where

$$k_s = \frac{2k_Ck_F}{k_C+k_F}. \tag{9}$$

If $k_C = k_F = k_s$, then

$$R_c^* = \left(\frac{1}{\pi}\right)\ln\left(\frac{1}{N^*}\right) - 0.7206. \tag{10}$$

2.2 Resistance of the gas-filled gap

The thermal resistance of the gas-filled gap depends on three local quantities: the separation of the two solid bounding surfaces, the thermal conductivity of the gas, and the temperature difference between the surfaces.

The gap is divided into elemental heat flow channels having isothermal upper and lower surfaces, and adiabatic sides (see fig. 1). The heat flow lines in each channel are assumed to be straight and perpendicular to the plane of contact, which is a reasonable assumption near the line contact where the two solid surfaces are

nearly parallel to the contact plane.

If the local gas conductivity, $k_g(x)$, in each elemental heat flow channel is assumed to be uniform across the local gap of thickness $\delta(x)$, then the differential heat flow through an elemental channel is

$$dQ_g = 2wk_g(x)\frac{\Delta T(x)}{\delta(x)}\,dx. \tag{11}$$

The total heat flow through the gas-filled gap, including gaps on both sides of the line contact, is given by the integral

$$Q_g = 4w\int_{x=b}^{D/2}\frac{k_g(x)\Delta T(x)}{\delta(x)}\,dx. \tag{12}$$

The thermal resistance of the gas-filled gap, R_g, is defined in terms of the temperature difference, ΔT_c, at the cylinder-flat contact:

$$\frac{1}{R_g} = \frac{Q_g}{\Delta T_c} = \frac{4w}{\Delta T_c}\int_{x=b}^{D/2}\frac{k_g(x)\Delta T(x)}{\delta(x)}\,dx. \tag{13}$$

The determination of local gap thickness, $\delta(x)$, for a cylinder and a flat in elastic contact must take into account the significant elastic deformation that occurs near the line contact under load. An expression for local gap thickness as a function of the normal load has been derived [6] and is given by

$$\delta(x) = \left[(D/2)^2 - b^2\right]^{1/2} - \left[(D/2)^2 - x^2\right]^{1/2} + \frac{4N\Delta}{2w\pi}\left\{\left(\frac{x}{b}\right)\left[\left(\frac{x}{b}\right)^2 - 1\right]^{1/2} - \left(\frac{x}{b}\right)^2 + 1 - \cosh^{-1}\left(\frac{x}{b}\right)\right\}. \tag{14}$$

Further details on the derivation of eq. (14) are given in Appendix A.

A model suggested by Kaganer [7] for the effective thermal conductivity of a gaseous layer contained between infinite parallel plates is used to determine the local conductivity in each elemental heat-flow channel as

$$k_g(x) = k_{g,\infty}\Big/\left(1 + \frac{\alpha\beta\Lambda}{\delta(x)}\right), \tag{15}$$

where $k_{g,\infty}$ is the conductivity of the gas under continuum conditions at STP. The accommodation parameter, α, is defined as

$$\alpha = \frac{2-\alpha_C}{\alpha_C} + \frac{2-\alpha_F}{\alpha_F}, \tag{16}$$

where α_C and α_F are the accommodation coefficients at the solid–gas interfaces. The fluid property parameter, β, is defined by

$$\beta = \frac{2\gamma}{\Pr(\gamma+1)}, \tag{17}$$

where γ is the ratio of specific heats, and Pr is the Prandtl number. The mean free path, Λ, of the gas molecules is given in terms of $\Lambda_{g,\infty}$, the mean free path at STP, as follows:

$$\Lambda = \Lambda_{g,\infty}(T_g/T_{g,\infty})(P_{g,\infty}/P_g). \tag{18}$$

Three models for calculating the local temperature difference, $\Delta T(x)$, were considered. In the first model it is assumed that the bounding surfaces are isothermal at their respective contact temperatures; hence

$$\Delta T(x) = \Delta T_c. \tag{19}$$

This is called the decoupled model, since it implies that the surface temperature at the solid–gas interface is independent of the temperature field within the solid.

In the second model, it is assumed that the temperature distribution at the solid–gas interface is induced by the heat flow through the solid–solid contact, under vacuum conditions [8]. This temperature distribution is approximated by the temperature field immediately below the surface of an insulated half-space that receives heat from an isothermal strip contact. Solving for this temperature field, using elliptic-cylinder coordinates, and transforming back to the Cartesian reference frame (see Appendix B), yields

$$\Delta T(x) = \frac{2Q_c\cosh^{-1}(x/b)}{2w\pi k_s}. \tag{20}$$

Since the solid–gas interface temperature is coupled to the interior temperature field of a half-space, eq. (20) is called the half-space model temperature drop.

The third approach assumes that the temperature distribution at the solid–gas interface is induced by linear heat flow through narrow, parallel heat-flux channels in both the solid and gaseous regions [9]. The local temperature drop is in proportion to the total joint temperature drop as is the fluid resistance to the total resistance, which gives

$$\frac{\Delta T(x)}{\Delta T_o} = \left[\frac{k_g(x)D}{k_s\delta(x)} + \left(1 - \frac{k_g(x)}{k_c}\right)\right]^{-1} \tag{21}$$

after algebraic manipulation of the elemental resistances, as described in Appendix B. This is referred to as the parallel flux-tube model.

Three models for the thermal resistance of the gas-filled gap can now be formulated by combining the formulae for the local gap thickness, $\delta(x)$, and the thermal conductivity of the gaseous region, $k_g(x)$, with the three expressions for the local temperature drop, $\Delta T(x)$.

2.2.1. Decoupled model (DCM)

From eq. (19), the local temperature drop for the DCM is simply $\Delta T(x) = \Delta T_c$, and substituting this, together with eqs. (14) and (15), into eq. (13) yields, for the gap thermal resistance, in nondimensional form,

$$\frac{1}{R_g^*} = \frac{2k^*}{L} I_1(L, M), \tag{22}$$

where $I_1(L, M)$ is the integral $\int_{\xi=1}^{L} \Phi(L, M, \xi)\mathrm{d}\xi$ and

$$\Phi(L, M, \xi) = \frac{1}{\delta^*(L, \xi) + M}. \tag{23}$$

The nondimensional parameters are defined as

$$\xi = \frac{x}{b}, \quad k^* = \frac{k_{g,\infty}}{k_s}, \quad \delta^*(L, \xi) = \frac{2\delta(x)}{D}$$

$$\text{and } M = \frac{2\alpha\beta\Lambda}{D},$$

where

$$\delta^*(L, \xi) = \left(1 - \frac{1}{L^2}\right)^{1/2} - \left(1 - \frac{\xi^2}{L^2}\right)^{1/2} + \frac{1}{2L^2}\left[\xi(\xi^2 - 1)^{1/2} - (\xi^2 - 1) - \cosh^{-1}(\xi)\right]. \tag{24}$$

2.2.2. Half-space model (HSM)

Substituting eq. (20), the local temperature drop for the HSM, into eq. (13), together with eqs. (14) and (15), yields, for the gap thermal resistance, in nondimensional form,

$$\frac{1}{R_g^*} = \frac{2k^*}{L} I_2(L, M), \tag{25}$$

where $I_2(L, M)$ is the integral $\int_{\xi=1}^{L} X(L, M, \xi)\mathrm{d}\xi$ and

$$X(L, M, \xi) = \frac{2\cosh^{-1}(\xi)}{\pi R_c^*(L)[\delta^*(L, \xi) + M]}. \tag{26}$$

2.2.3. Parallel flux-tube model (PFTM)

For the PFTM, the local temperature drop is given by eq. (21) and when this is substituted in eq. (13), together with eqs. (14) and (15), the gap thermal resistance, in nondimensional form, is

$$\frac{1}{R_g^*} = \frac{2k^*}{L} I_3(L, M, k^*), \tag{27}$$

where $I_3(L, M, k^*)$ is the integral $\int_{\xi=1}^{L} \Psi(L, M, k^*, \xi)\mathrm{d}\xi$ and

$$\Psi(L, M, k^*, \xi) = \frac{\Delta T_o}{\Delta T_c}\left[\delta^*(L, \xi)\left(1 - k^*\frac{k_s}{k_c}\right) + 2k^* + M\right]^{-1}. \tag{28}$$

The functions $\Phi(L, M, \xi)$, $X(L, M, \xi)$ and $\Psi(L, M, k^*, \xi)$ describe the heat flow across the gas-filled gap for each model. These functions were evaluated numerically, and are plotted in figs. 2, 3 and 4 as a function of distance from the contact line, for a range of values of the fluid parameter, M.

For small values of M, corresponding to gas pressures near one atmosphere, there are distinct differences between the models with respect to the contribution to gaseous heat flow near the contact line. In this region, the DCM and HSM predict very large heat flows, which will tend to dominate the contribution from solid-to-solid heat transfer. The heat flow predicted by the PFTM in the vicinity of the contact is much smaller than for the other two models and is of the same magnitude as the solid-to-solid heat flow.

At low gas pressures, i.e., larger values of M, differences in the values of the integrals tend to disappear, and all three models predict about the same amount of heat flow over the entire gap. Again, the major differences occur near the line contact, but the values quickly flatten out and decrease, so that at low gas pressures solid-to-solid conduction dominates.

2.3. Total joint resistance

In combining the constriction resistance, due to line contact, with the resistance of the gas-filled gap, it is assumed that the respective heat flows are independent, so that the dimensionless resistances may be summed in parallel as

$$\frac{1}{R_j^*} = \frac{1}{R_c^*(N^*)} + \frac{1}{R_g^*(L, M, k^*)}. \tag{29}$$

For the purposes of this analysis the thermal radiative resistance is assumed to be large and is not considered.

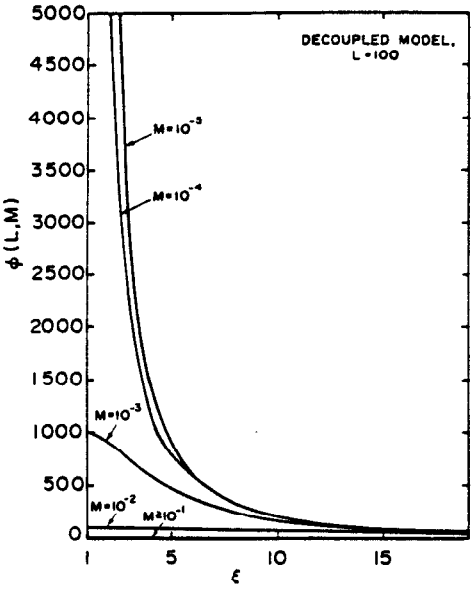

Fig. 2. Local variation in gaseous heat flow for decoupled model.

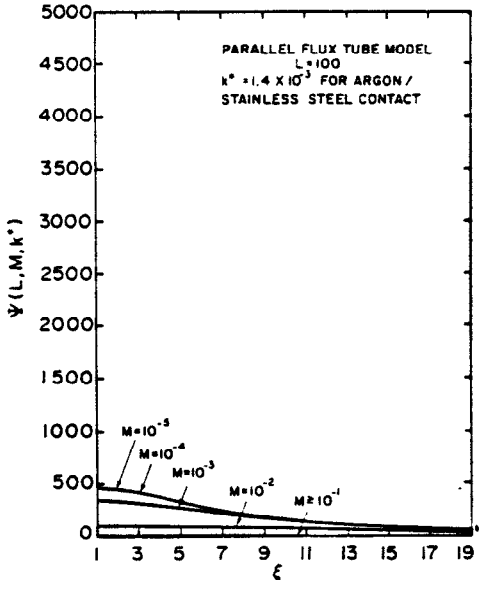

Fig. 4. Local variation in gaseous heat flow for parallel flux-tube model.

The above analysis has expressed the total dimensionless joint resistance in terms of four important geometrical and thermophysical parameters: a contact parameter L, a dimensionless load parameter N^*, a fluid property parameter M, and a thermal conductivity ratio k^*. Their roles in controlling heat flow across a cylinder-flat joint are summarized in table 1.

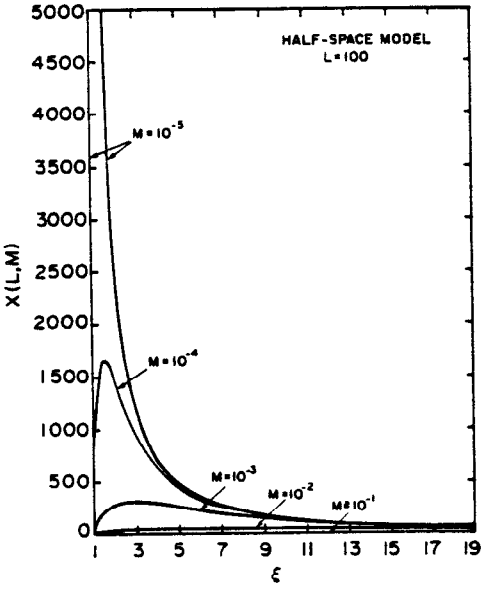

Fig. 3. Local variation in gaseous heat flow for half-space model.

2.4. Experimental verification

A series of experiments was performed to test the validity of the theoretical models and also to enhance our understanding of the mechanisms controlling the resistance to heat transfer across a cylinder-flat joint. Thermal experiments were performed on several materials (tool steel, stainless steel, and zirconium alloys) in vacuum and in helium and argon atmospheres at pressures up to atmospheric.

2.4.1. Test apparatus and specimens

The test apparatus, shown schematically in fig. 5, consisted of a stainless-steel vacuum vessel, a mechanical loading apparatus, and a vacuum system. A normal load was applied to the test column by a second-class lever, with hanging weights. Up to 25 W of heat was supplied to the test column with a cartridge heater, located in a close fitting hole in the upper specimen. The lower specimen was cooled at its base by a flow of cold water through a heat sink maintained at a temperature of $(9.5 \pm 0.5)°C$ for the duration of each experiment.

Table 1
Summary of thermal joint resistance parameters

Definition	Description
$L = D/2b$	Dimensionless contact parameter
$N^* = \frac{N\Delta}{2wD} = \frac{\pi}{16L^2}$ where $\Delta = \frac{1}{2}\left(\frac{1-\nu_C^2}{E_C} + \frac{1-\nu_F^2}{E_F}\right)$	Accounts for effects of normal load, elastic properties and geometry
$M = 2\alpha\beta\Lambda/D$ where $\alpha = \frac{2-\alpha_C}{\alpha_C} + \frac{2-\alpha_F}{\alpha_F}$, $\beta = 2\gamma/\mathrm{Pr}(\gamma+1)$, $\Lambda = \Lambda_{g,\infty}\left(\frac{T_g}{T_{g,\infty}}\right)\left(\frac{P_{g,\infty}}{P_g}\right)$	Represents fluid condition: accounts for effects of solid/fluid molecular accomodation, fluid temperature and pressure, and fluid transport properties
$k^* = \frac{k_{g,\infty}}{k_s}$	Ratio of fluid free-stream thermal conductivity to harmonic mean of thermal conductivities of contacting solids. It characterizes the relative importance of conduction through solid and fluid

The test column consisted of a half-cylinder (lower specimen) in contact with a flat (upper specimen). The flat surface of the upper specimens was produced by finish grinding, which produced an exceptionally flat surface with acceptable roughness. The Zircaloy-4 and Keewatin tool steel cylinders were produced by centreless grinding to the desired diameter. The full cylinder was then cut to produce a half-cylinder that could be mounted against a flat-topped base (lower specimen), made from the same material. The stainless-steel cylinder was turned and honed, and then mounted in a cylindrical groove in the top of a Type 304 stainless steel base. Surface roughness values of the contacting surfaces, made with the WNRE surface roughness measurement system [10], are reported in table 2.

Eight thermocouples were attached to each specimen. Their axial positions, measured using a travelling microscope, are shown in fig. 6. The thermocouple leads were wrapped around the specimens to reduce the "fin effect", and securely fastened with small straps. Each junction was covered with a ceramic cement and the test column was wrapped in a 20 mm thick blanket of quartz wool insulation and then covered with an aluminum foil to reduce radial heat losses. Specimen material properties and dimensions are given in table 2.

Tests were conducted in ultra-high purity argon and helium, at controlled pressures ranging from 10^{-7} to

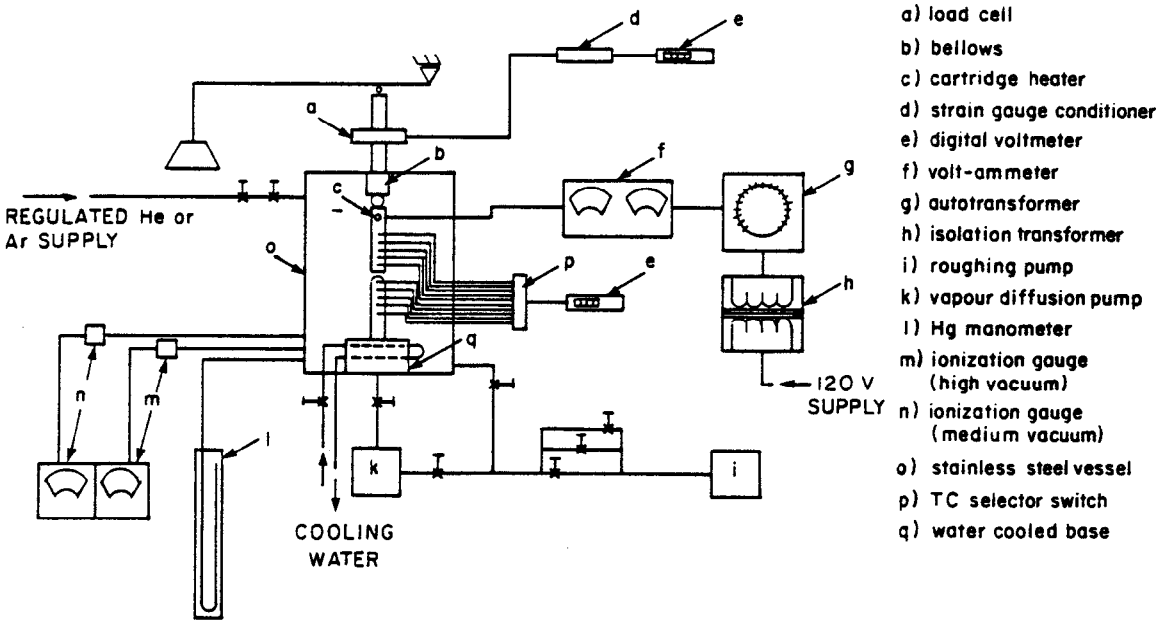

Fig. 5. Schematic of test apparatus.

Table 2
Specimen properties and dimensions [a]

Property	Keewatin Tool Steel	304 Stainless Steel	Zircaloy-4
k(W/(m K))	$34.13-(1.7993E-3)T$	$10.67+(1.59E-2)T$	$7.51+(2.09E-2)T-(1.45E-5)T^2$
E(GPa)	$228.8-(7.6E-2)T$	$207.5-(7.6E-2)T$	$117.11-(6.7E-2)T$
ν	0.3	0.3	$0.333-(1.261E-4)T$
Hardness	R_c60	R_b75	R_b94
Roughness			
Cyl.: $\sigma(\mu m)$	0.464	0.339	0.607
m(rad)	0.110	0.070	0.230
Flat: $\sigma(\mu m)$	0.111	0.117	1.372
m(rad)	0.027	0.022	0.090
Dimensions			
D(mm)	25.4	20.0	25.4
$2w$(mm)	25.4	40.0	25.4

[a] Notes: Temperatures (T) in Kelvin, σ – RMS roughness height, m – mean asperity slope.

740 Torr. The thermophysical properties of these gases are given in table 3.

2.4.2. Test procedure and data reduction

Two types of contact-resistance tests were performed. In the first, the pressure was maintained as low as possible (below 10^{-5} Torr), and measurements were made with various values of applied contact load between 80 N and 8000 N. In the second, the load was held constant while the fluid pressure was varied between 10^{-7} Torr and 740 Torr.

For each test, the input conditions (e.g., load, fluid pressure, heater power) were maintained until the specimen temperature profile became steady.

The temperature readings from a typical test are plotted in fig. 6. A linear representation of the temperature measurements in the upper and lower specimens of the form

$$T = a + bz \tag{30}$$

was determined, using a least-squares regression. These temperature profiles were extrapolated to the plane of contact, and the difference between the extrapolated values was taken as the contact temperature drop. A simple differential error analysis of the formulae used to compute the slope, intercept and extrapolated tempera-

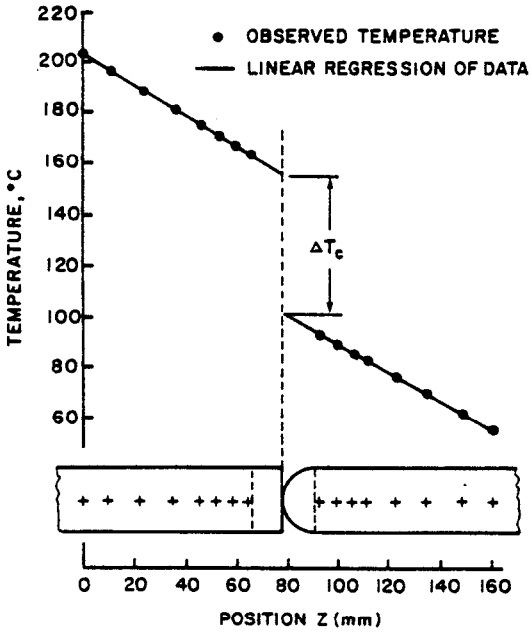

Fig. 6. Typical temperature profile for test column.

Table 3
Thermophysical properties of cases [a]

Property	Argon	Helium
$k_{g,\infty}$(W/(m K))	$4.764E-3+(4.364E-5)T$	$5.282E-2+(3.602E-4)T$
$\Lambda_{g,\infty}$(pm)	66.6	186.2
γ	1.667	1.667
Pr	0.667	0.667
α	0.6	0.4

[a] Note: Λ values are for 288 K, 760 Torr.

tures showed that a random error of ±1.5% due to thermocouple inaccuracy may be expected in the computed resistance.

The termal conductivities of the upper and lower specimens were evaluated at the interpolated temperatures of the mid-planes of these conductors. Based on these conductivities, the source and sink heat flow rates were computed from

$$Q = -kbD2w, \tag{31}$$

where b is the thermal gradient defined by eq. (30).

The heat flow rate in the lower specimen, or sink, was used as the heat flow rate across the contact plane, and the experimental joint resistance was determined as

$$R_{j,exp} = \Delta T_c / Q. \tag{32}$$

The thermal conductivity at each of the extrapolated contact temperatures was then evaluated. The harmonic mean of these conductivities was taken as k_s, and the dimensionless experimental resistance was computed as

$$R^*_{j,exp} = 2wk_s R_{j,exp}. \tag{33}$$

An overall random error of ±5% was considered a reasonable estimate of measurement uncertainty.

It is assumed that, under vacuum conditions, the total joint resistance consists of only constriction and radiation components. The radiative resistance was calculated to be about 200 times larger than the constriction resistance, so that the bulk of the heat flow (> 99,5%) in vacuum is by conduction through the line contact. If it is also assumed that these two components remain constant as the fluid pressure increases, then the measured fluid resistance may be estimated by subtraction of the vacuum and non-vacuum values of the total resistances, i.e.,

$$R^*_{g,exp} = \left(\frac{1}{R^*_{j,exp}(M, N^*)} - \frac{1}{R^*_{c,exp}(M \to \infty, N^*)} \right)^{-1}, \tag{34}$$

where N^* is the dimensionless load parameter and M is the fluid property parameter. Large values of M imply low fluid pressure and $M \to \infty$ is the vacuum condition.

Other properties, such as fluid mean free path and Young's modules, were evaluated at the contact temperature, taken as the arithmetic mean of the two extrapolated temperatures.

Using the above procedure, a FORTRAN computer program was written to compute the measured resistances and compare them with the predictions of the theoretical models.

3. Results

3.1. Tests in vacuum

The resistances measured in vacuum for Zircaloy-4, Keewatin tool steel and Type 304 stainless steel are compared with the model predictions in fig. 7. At light loads ($N^* < 5 \times 10^{-6}$), agreement with the predictions of the line-contact model is poor, particularly for the centreless-ground Zircaloy-4 and Keewatin tool steel specimens. The higher resistances measured at light loads are attributed to errors of form (crowning) along the longitudinal contact line of the semi-cylinder. Rather than the long rectangular contact of the ideal case, a slight error of form results in a small elliptical contact that gives a much greater constriction to heat flow.

As the load increases, error-of-form effects are overcome as the elliptical contact grows into a long rectangular strip. For $N^* \geq 5 \times 10^{-6}$, the measured resistances are in good agreement with the predictions of the line-contact model.

3.2. Tests in fluid

The variation of joint resistance with fluid pressure was investigated for both helium and argon gas, using the stainless-steel samples. Fluid pressure was varied from vacuum ($M \sim 10^5$–10^6) to atmospheric pressure ($M \sim 10^{-3}$), while a constant normal load was maintained across the contact. Results measured in helium with the load maintained at 2700 N ($N^* = 1.8 \times 10^{-5}$) are shown in fig. 8. The dimensionless joint resistance decreased from 2.5 to 1.5 as helium pressure increased from vacuum to atmospheric. Very little change in resistance occurred until the fluid parameter M approached

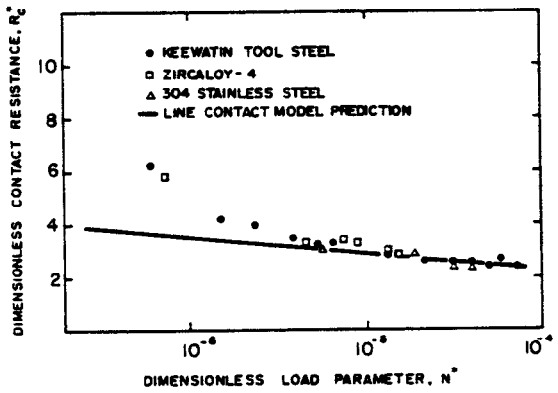

Fig. 7. Variation of resistance with load in vacuum.

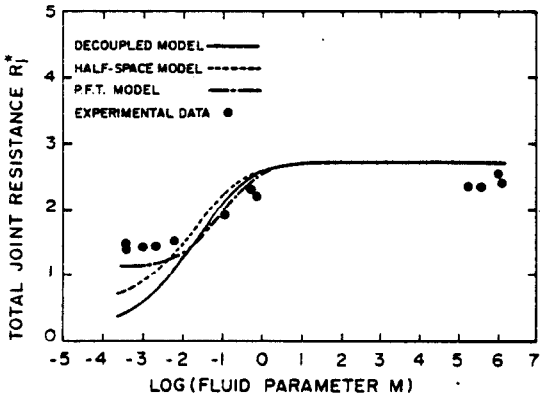

Fig. 8. Variation of total joint resistance with M; $N^* = 1.8 \times 10^{-5}$, helium.

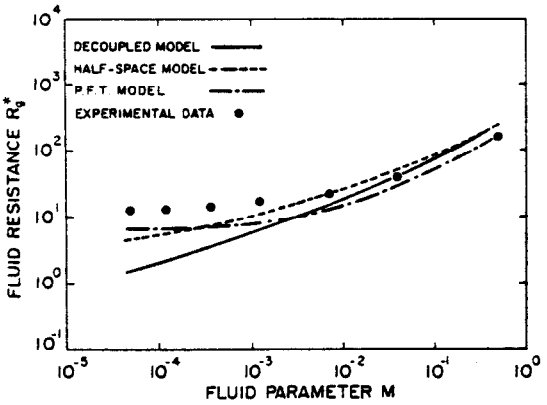

Fig. 11. Variation of fluid resistance with M; $N^* = 1.8 \times 10^{-5}$, argon.

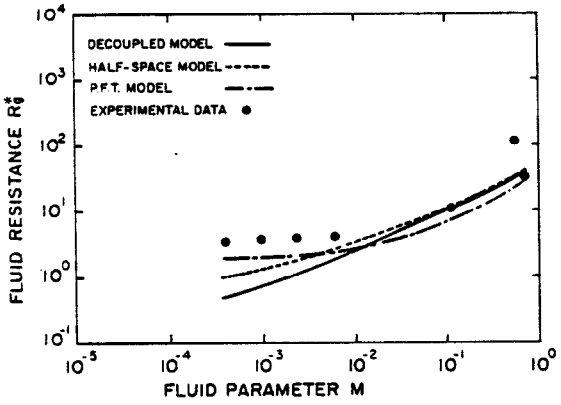

Fig. 9. Variation of fluid resistance with M; $N^* = 1.8 \times 10^{-5}$, helium.

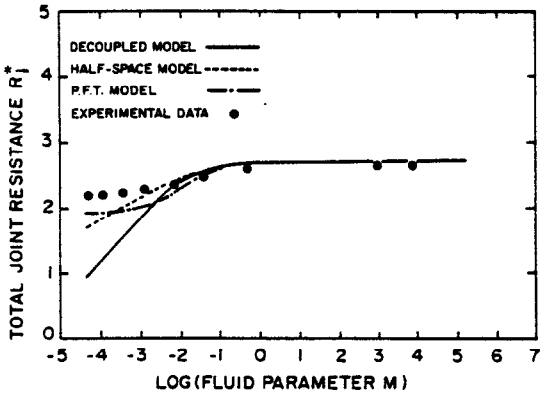

Fig. 10. Variation of total joint resistance with M; $N^* = 1.8 \times 10^{-5}$, argon.

1, corresponding to a pressure of 10^{-3} Torr. The resistance decreased noticeably between $M = 1$ and $M = 10^{-2}$ and then levelled out below $M = 10^{-2}$ as the helium pressure approached atmospheric. The theoretical predictions of joint resistance are also plotted in fig. 8. The observed trends, particularly near atmospheric pressure, tend to favour the parallel flux-tube model.

The experimental gap resistance, $R^*_{g,exp}$, obtained from eq. (34) is compared in fig. 9 with the predictions of the three gap-resistance models. Near atmospheric pressure, the measured gap resistances are independent of fluid pressure, and the predictions of the PFTM are in fair agreement with this observed trend.

A similar experiment was performed in argon, which has a lower thermal conductivity than helium. The results, shown in fig. 10, indicate that the joint resistance is not very sensitive to changes in pressure over the observed range of the fluid parameter M. This result is predicted by the theoretical models, for a fluid of poor thermal conductivity, since a large fraction of the heat flows through the solid contact.

Comparison of the experimental gap resistance in argon with model predictions is shown in fig. 11, and at low pressures ($10^{-2} \leq M \leq 1$) all three models are in fair agreement with the experimental results. Near one atmosphere the experimental gap resistance is independent of fluid pressure and follows the trend predicted by the PFTM.

4. Discussion

Thermal contact resistance measurements in vacuum indicate that, at light loads, slight crowning or out-of-

flatness leads to large discrepancies between the measured resistances and the predictions of the line-contact model. Profilometer measurements [10] indicate that this crowning was typically 1–3 μm over the length of the cylinder. At the lightest loads this crowning will result in contact over a small elliptical area, with the semi-major axis parallel to the axis of the cylinder. This contact geometry provides much greater constriction to heat flow than the ideal line contact, at the same load. As the load is increased, the ellipse grows and changes shape until it becomes essentially the long narrow rectangular contact assumed in the theoretical analysis. In this range ($N^* > 5 \times 10^{-6}$) agreement with the line-contact model is very good, and the measured constriction resistance is fairly insensitive to further increases in load.

Experiments designed to measure the resistance to heat flow across the gap were not as conclusive in ascertaining the validity of the proposed models for fluid gap resistance. The experiments generally confirmed that the total joint resistance is more sensitive to fluid pressure with a high-conductivity fluid such as helium in the gap than with a low-conductivity fluid, such as argon. Resistances measured with $M < 10^{-2}$, i.e., near one atmosphere, are insensitive to changes in fluid pressure, and show qualitative agreement with the PFTM.

The DCM, HSM, and PFTM differ in the method for calculating the temperature drop across the joint. The DCM and HSM, originally developed for the more resistive sphere-flat contact geometry [8], imply that the ratio of the temperature drop across the contact to the total temperature drop, $\Delta T_c/\Delta T_o$, is near unity. However, values of $\Delta T_c/\Delta T_o$ as low as 0.6 were observed during our cylinder-flat joint resistance measurements. The PFTM implies that the thermal resistance associated with constriction through the contact is comparable to the resistance of the fluid gap, which could account for its better qualitative agreement with the measured values.

5. Conclusions and recommendations

Experimental measurements of the thermal resistance across a cylinder-flat contact in vacuum have confirmed the validity of the line-contact model, provided the contact load is sufficient to overcome the effects of small amounts of crowning, or out-of-flatness. Below a certain value of the load parameter $N^*(5 \times 10^{-6}$ in this experiment), the line-contact model is not valid due to these errors of form. Further work is required to analyze the constriction of heat flow through small elliptical contacts that form when waviness or out-of-flatness is present on the contacting cylindrical surface.

A weak argument could be made in favour of the parallel flux-tube model, since it appears to best represent the dependence of measured joint resistance on fluid pressure. It should be used with caution, however, since large differences between model and measurement were observed under certain conditions. Refinements to the fluid gap resistance model are required, particularly in the handling of the bounding surface temperature distribution.

Appendix A

A general expression for the surface separation between two contacting bodies is [11]

$$\delta(x) = \delta_0(x) - \alpha + w(x) - w_0 \tag{A1}$$

where

$$\delta_0(x) = \tfrac{1}{2}D - \left[(D/2)^2 - x^2\right]^{1/2} \tag{A2}$$

is the gap at zero load, determined from the cylinder-flat geometry, and

$$\alpha = \tfrac{1}{2}D - \left[(D/2)^2 - b^2\right]^{1/2} \tag{A3}$$

is the gap at $x = b$ at zero load. $w(x)$ is the surface deformation resulting from the applied load and w_0 is the compliance of the two bodies due to surface deformation.

The quantities w and w_0 are approximated by considering the deformation of the surface of a semi-infinite elastic solid due to a band of applied pressure. This gives [2,3]

$$w(x) = \frac{-2(1-\nu^2)}{\pi E}\int_{-b}^{b} N'\left[\ln(x-x') + k\right] \mathrm{d}x' \tag{A4}$$

where the Hertz pressure distribution is given by:

$$N' = N_0\left[1 - (x'/b)^2\right]^{1/2}, \quad -b < x' < b$$

and k is a constant. The integral of eq. (A4) contains a pole at $x = x'$; the integration must be performed along a path that avoids this point. A transformation to the complex plane, and a series expansion of the resulting integrand, yields

$$w(x) = \frac{(1-\nu^2)}{E} N_0 b \left\{ \left(\frac{x}{b}\right)\left[\left(\frac{x}{b}\right)^2 - 1\right]^{1/2} - \cosh^{-1}\left(\frac{x}{b}\right) - \left(\frac{x}{b}\right)^2 + k \right\} \tag{A5}$$

outside the contact ($|x| > b$), and

$$w(x) = \frac{(1-\nu^2)}{E} N_0 b \left[k - \left(\frac{x}{b}\right)^2 \right] \tag{A6}$$

within the contact ($|x| < b$), with k being an integration constant. From a force balance, the maximum pressure is

$$N_0 = 2N/2wb\pi. \tag{A7}$$

By means of eqs. (A5)–(A7), the contact size (eq. (1)) may be derived. The displacement described by eq. (A5) occurs on both contacting surfaces; therefore

$$w(x) = \frac{4N\Delta}{2w\pi} \left\{ \left(\frac{x}{b}\right) \left[\left(\frac{x}{b}\right)^2 - 1 \right]^{1/2} - \cosh^{-1}\left(\frac{x}{b}\right) - \left(\frac{x}{b}\right)^2 + k \right\} \tag{A8}$$

and

$$w_0 = w(b) = \frac{4N\Delta}{2w\pi}(k-1). \tag{A9}$$

Substitution of eqs. (A2), (A3), (A8) and (A9) into (A1) yields:

$$\delta(x) = \left[\left(\frac{D}{2}\right)^2 - b^2 \right]^{1/2} - \left[\left(\frac{D}{2}\right)^2 - x^2 \right]^{1/2} + \frac{4N\Delta}{2w\pi} \left\{ \left(\frac{x}{b}\right) \left[\left(\frac{x}{b}\right)^2 - 1 \right]^{1/2} - \cosh^{-1}\left(\frac{x}{b}\right) - \left(\frac{x}{b}\right)^2 + 1 \right\} \tag{A10}$$

or

$$\delta^*(\xi) = \frac{2\delta(x/b)}{D} = \left[1 - \left(\frac{1}{L}\right)^2 \right]^{1/2} - \left[1 - \left(\frac{\xi}{L}\right)^2 \right]^{1/2} + \frac{1}{2L} \left[\xi(\xi^2-1)^{1/2} - \cosh^{-1}(\xi) - \xi^2 + 1 \right]. \tag{A11}$$

Appendix B. Half-space model

The half-space shown in fig. B1(a) will be used to approximate the temperature field inside the cylinder or flat block. It receives heat at a rate Q_c from an isothermal strip contact at temperature T_c. The isotherms and adiabats conform to the elliptic-cylinder coordinate system, so this temperature field may be described by the

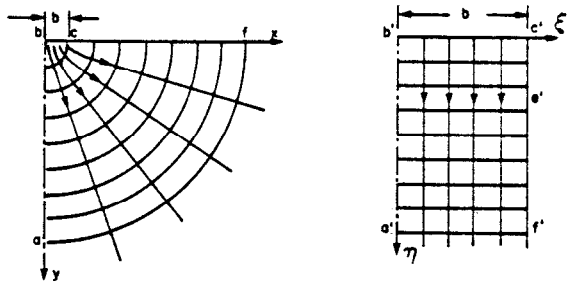

Fig. B1. (a) Temperature field in half-space (b) Temperature field in transformed complex plane.

linear relationship $T = A\eta + B$(fig. B1(b)). From the stated boundary (contact) conditions, $B = T_c$ and $A = -Q_c/(2wk\pi)$. Thus,

$$T = \frac{Q_c \eta}{2wk\pi} + T_c. \tag{B1}$$

From the transformation relations for the elliptic-cylinder coordinate system [12], we find that, along the solid surface ($y = 0$), $\eta = \cosh^{-1}(x/b)$. This temperature field is imposed upon both of the contacting bodies; thus,

$$\Delta T(x) = \frac{2Q_c \cosh^{-1}(x/b)}{\pi k_s 2w}, \tag{B2}$$

where k_s is the harmonic mean thermal conductivity.

Parallel flux-tube model

If we were to divide the entire cylinder-flat joint region into a series of parallel flux-tubes, then, considering the heat transfer by conduction from the hot upper surface, through the cylinder, the fluid, and the flat block to the cool lower surface (see fig. B2), we could write the resistance of these three components as

Cylinder:

$$R'_C = \frac{D/2 - \delta(x)}{k_C 2w\,dx}.$$

Fluid:

$$R'_g = \frac{\delta(x)}{k_g(x) 2w\,dx}. \tag{B3}$$

Flat:

$$R'_F = \frac{D/2}{k_F 2w\,dx}.$$

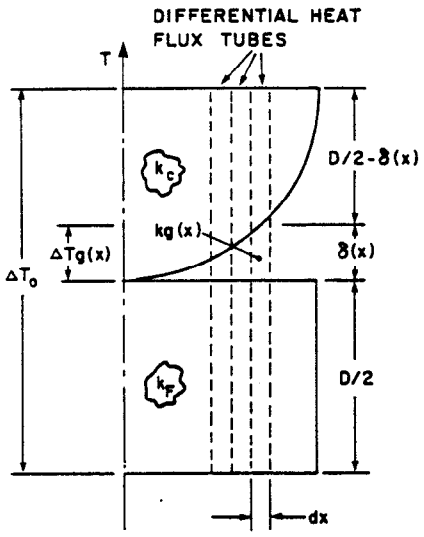

Fig. B2. Parallel flux-tube model geometry.

Note that the primes indicate that these resistances apply only to the differential flux-tubes. The portion of the total resistance of each flux-tube that is due to the fluid will be directly related to the temperature drop across the fluid, since conduction in each component is linear, i.e.,

$$\frac{\Delta T_g(x)}{\Delta T_o} = \frac{\delta(x)/(k_g(x)2w\mathrm{d}x)}{\dfrac{D/2-\delta(x)}{k_C 2w\mathrm{d}x} + \dfrac{\delta(x)}{k_g(x)2w\mathrm{d}x} + \dfrac{D/2}{k_F 2w\mathrm{d}x}}$$

$$= \left[\frac{k_g(x)D}{k_s \cdot \delta(x)} + \left(1 - \frac{k_g(x)}{k_C}\right)\right]^{-1}, \qquad \text{(B4)}$$

or

$$\frac{\Delta T_g(\xi)}{\Delta T_c} = \left[\frac{2k_g(\xi)}{k_s \cdot \delta^*(\xi)} + \left(1 - \frac{k_g(\xi)}{k_C}\right)\right]^{-1} \cdot \frac{\Delta T_o}{\Delta T_c}. \qquad \text{(B5)}$$

If $k_C = k_F = k_s$, then

$$\frac{\Delta T_g(\xi)}{\Delta T_c} = \left[\left(\frac{2}{\delta^*(\xi)} - 1\right)\frac{k_g(\xi)}{k_s} + 1\right]^{-1} \cdot \frac{\Delta T_o}{\Delta T_c}. \qquad \text{(B6)}$$

Acknowledgements

The authors acknowledge the assistance of Mr V.D. Kroeger in obtaining the experimental data and Mr D.W. Patterson in analyzing the data for Zircaloy-4.

Nomenclature

D cylinder diameter (m)
E Young's modulus (Pa)
L contact parameter, defined as $D/2b$
M fluid property parameter, defined as $2\alpha\beta\Lambda/D$
N total contact load (N)
N^* dimensionless load parameter, defined as $N\Lambda/2wD$
P pressure (Pa)
Pr Prandtl number
Q heat flow rate (W)
R thermal resistance (K/W)
R^* dimensionless thermal resistance, defined as $2wk_sR$
T temperature (K)
b line contact half-width (m), or thermal gradient (K/m), in context
k thermal conductivity (W/(m K))
k^* dimensionless fluid thermal conductivity, defined as $k_{g,\infty}/k_s$
w cylinder or flat half-length (m)
x fluid gap coordinate (m)

Greek letters

Δ effective combined elastic modulus, defined as

$$\frac{1}{2}\left(\frac{1-\nu_C^2}{E_C} + \frac{1-\nu_F^2}{E_F}\right)(\mathrm{Pa}^{-1})$$

Λ fluid molecular mean free path (m)
Φ integrand, defined by eq. (23)
X integrand, defined by eq. (26)
Ψ integrand, defined by eq. (28)
α solid–fluid accomodation coefficient
β fluid property parameter, defined as $2\gamma/\mathrm{Pr}(\gamma+1)$
γ ratio of specific heats
δ separation of cylinder and flat surfaces (m)
δ^* normalized surface separation, defined as $2\delta/D$
ν Poisson's ratio
ξ dimensionless gap coordinate, defined as x/b

Subscripts

C cylinder
F flat
c constriction
g fluid or gap
∞ continuum conditions
o overall
s harmonic mean value
j total joint
exp experimental value

References

[1] D.A. Meneley and W.T. Hancox, LOCA consequence predictions in a CANDU-PHWR, Report IAEA-CN-42/145, presented at the IAEA Int. Conf. on Nuclear Power Experience, Vienna (September 1982).

[2] S. Timoshenko and J.N. Goodier, Theory of Elasticity, 2nd ed. (McGraw-Hill , New York, 1951).

[3] J.A. Walowit and J.N. Anno, Modern Developments in Lubrication Mechanics (Applied Science Publishers, Barking, Essex, 1975).

[4] M.M. Yovanovich and J. Coutanceau, Sur al dètermination de la resistance thermique tranversale d'un cylindre de revolution homgène isotrope avec des conditions aux limites mixtes, C.R. Acad. Sci. Paris 268 (1969) B821-B823.

[5] T.N. Veziroglu and S. Chandra, thermal conductance of two-dimensional contrictions, in: Thermal Design Principles of Spacecraft and Entry Bodies, Prog. Astronautics and Aeronautics, Vol. 21, ed., J.T. Bevans (AIAA, New York, 1969) pp. 591-651.

[6] G.R. McGee, An Analytical and Experimental Study of the Heat Transfer Characteristics of Cylinder-Flat Contacts, M.A.Sc. thesis (University of Waterloo, 1982).

[7] M.G. Kaganer, Thermal Insulation in Cryogenic Engineering, translated from Russion by A. Moscona (Israel Program for Scientific Translations, Jerusalem, 1969).

[8] Y. Ogniewicz and M.M. Yovanovich, Effective conductivity of regularly racked sphers: basic cell model with contriction, in: Heat Transfer and Thermal Control Systems, Progress in Astronautics and Aeronautics, Vol. 60, ed., L.S. Fletcher (AIAA, New York, 1978) pp. 209–228.

[9] D. Kunii and J.M. Smith, Heat transfer characteristics of porous rocks, AIChe J. 6, No. 1 (1960) pp. 71–78.

[10] F. Hughes and M.H. Schankula, A computer-aided surface roughness measurement system, Whiteshell Nuclear Research Establishment, AECL-6829 (November 1983).

[11] A. Cameron, Principles of Lubrication (Wiley, New York, 1966) Ch. 8.

[12] M.M. Yovanovich, Advanced Heat Conduction (Hemisphere Publishing, Washington), to be published.